1

Real-Time Colour Holographic Interferometry (from Holographic Plate to Digital Hologram)

Jean-Michel Desse
Office National d'Etudes et Recherches Aérospatiales (ONERA) Lille
France

1. Introduction

In the area of Fluids Mechanics, detailed analysis and characterization of complex, unsteady flows require non-invasive optical methods to measure smaller and smaller quantities over space or time, or even both at once. Therefore, many researchers have spent considerable time over the last fifty years to develop metrology tools adapted to quantitative flow visualization. Some of these methods such as shadowgraph or schlieren method are based on measuring the light deviation through the test section (Merzkirch, 1974), other methods such as interferometry or holography are based on optical interferences and on measurement of the optical path difference or the signal phase (Vest, 1979). When qualitative measurements of the flow are sought, the former techniques can be used. The concepts and the many applications of shadowgraph or schlieren techniques can be found in (Settles, 2001). If quantitative data are required, Mach-Zehnder or Michelson interferometers have been developed, but these instruments are very sensitive to external vibrations, especially when the two arms of the interferometer have unequal length (Merzkirch, 1974). To avoid this problem, differential interferometry or Wollaston-prism shearing interferometry using a polarized white light source can be implemented (Philbert, 1958; Merzkirch, 1965; Smeets, 1975), but these techniques visualize the first derivative of the refractive index in the test section. The same optical technique equipped with high speed camera can be also used to analyze high speed flows (Desse, 1990, 2006). In this case, a sequence of colour interferograms is recorded at a high framing rate from which the derivative of the gas density can be extracted. The interferograms are analyzed nearly automatically by an image processing software specially designed for modelling the light intensity of the interference fringes as the path difference varies (Desse, 1997a). As the method gives a differential measurement, integration is necessary to get the full gas density field, whence a certain imprecision arises in the measurements. To avoid such imprecision related to integration and to maintain the advantage of colour interferograms[1], real-time colour holographic interferometry has been developed. One of the two variants of colour holographic interferometry is perfectly suitable for analyzing unsteady aerodynamic

[1] Colour interferometry has the property to exhibit a unique white fringe visualizing the zero order of interferences

phenomena (i.e., of transparent objects) and for real-time analysis of mechanical deformations (diffusive objects). The usual double-exposure method consists in recording the holograms of a transparent or diffusive object in two different states in succession, on the same photographic plate. This proven technique has yielded good results for several years, but it does have the disadvantage of not allowing the interferogram of the phenomenon being studied to be observed immediately and without interruption. Real-time colour holographic interferometry, on the other hand, allows direct observation through a reference hologram and makes it possible to take an ultra-high speed movie of the interferogram of a changing phenomenon (Surget, 1973). This was the method used.
After presenting the advantages associated with the use of a polychromatic light source rather than monochromatic, the principles of three-wavelength holographic interferometry in real-time are detailed. The feasibility of the method is shown when silver-halide panchromatic holographic plates are used either in transmission or reflection. The advantages and disadvantages of these techniques for recording and reconstruction, though substantially different, are presented through an application that examines the unsteady wake flow downstream of a cylinder at a subsonic Mach number. To conclude this chapter, colour digital holographic interferometry is presented as a method preferable to holographic techniques using holographic plates even if the new generation of CMOS or CCD sensors are far from having the spatial resolution of holographic plates.

2. Advantage of using one source to multiple wavelengths

In monochromatic interferometry (for instance, λ=647nm), it is well known that the classical interference pattern is represented by a succession of dark and bright red fringes. For two successive fringes, the optical path difference is equal to the wavelength of the laser source (Fig.1a). Unfortunately, the zero order of interferences fringes can never be identified and it

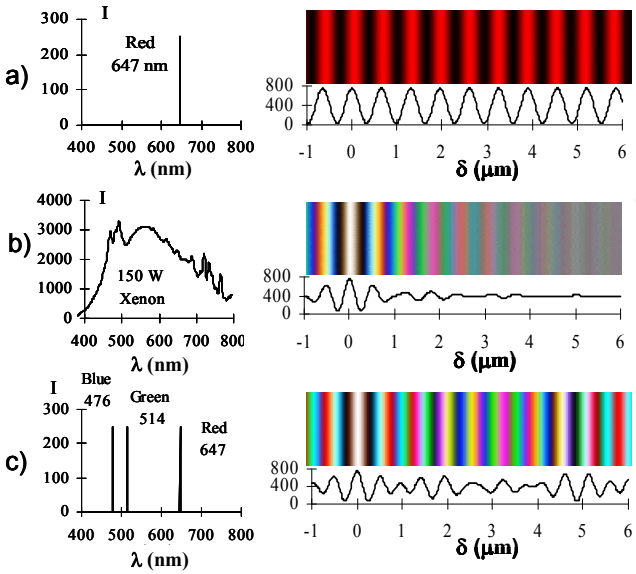

Fig. 1. Spectra and interference fringes given by three different light sources

is one of the major difficulties with interferences fringes in monochromatic light. Sometimes, it is not possible to follow the displacement of the fringes through a shock wave, for example, or to count the fringe number in a complex flow. When the light source is a continuous source (500 Watt xenon, see Fig. 1b), the interference pattern is a coloured fringe pattern in a sequence approximately matching Newton's colour scale. This fringes diagram exhibits a unique white fringe, visualizing the zero order of interference and it allows one to measure very small path differences, because six or seven different colours define the interval 0-0.8 microns. But, when the path difference is greater than three or four microns, the colours can no longer be separated and the larger path differences cannot be correctly measured (Desse, 1997b). Fig. 1c shows the fringes obtained with a laser that emits three different wavelengths (one blue line, one green line and one red line). One can see that the disadvantages of the two others sources have disappeared. The zero order is always identifiable and the colours always remain distinguishable for the small and the large path differences. The interference pattern also presents the following peculiarity: while the white fringe is not visible on the interferogram, the sequence of three successive colours in the diagram is unique.

3. Principle of real-time colour holographic interferometry

The various holographic interferometry methods – double exposure, time-averaged, or real-time holography – are the main scientific applications of holography. Until recent years, experiments in holographic interferometry were performed with a single laser, i.e., they were monochromatic. Most experiments found in the literature relate to transmission holograms (Rastogi, 1994) and few experiments have been performed to date using holographic interferometry with reflected white light (Smigielski et al., 1976; Vikram, 1992). It should be said that, in monochromatic mode, experiments in reflected white-light holography have little advantage over holographic interferometry in transmitted light. Some publications mention the use of three-wavelength differential interferometry (Desse, 1997b) and holographic interferometry by reflection (Harthong, 1997; Jeong, 1997) and all show that the essential advantage of colour is that the achromatic fringe can be located in the observed field.

Real-time true colour holographic interferometry uses three primary wavelengths (red, green, blue) to record the interference between the three object beams and the three reference beams simultaneously on a single reference hologram. Under no-flow conditions, the undisturbed object waves ΣRO, ΣGO and ΣBO are recorded in the hologram by virtue of their interference with the three reference waves ΣRR, ΣGR and ΣBR. As can be seen in Fig. 2, step 1, at recording and for a plate recorded in transmission, the three reference waves and the three object waves arrive on the same side of the plate while in reflection, they come from opposite sides of the holographic plate. After treatment of the plate and resetting in the optical bench, the three reference waves ΣRR, ΣGR and ΣBR are diffracted by transmission or by reflection according to the recording mode used to form the three diffracted object waves ΣROD, ΣGOD and ΣBOD (Step 3, Fig. 2).

Then the hologram is illuminated simultaneously by the three reference beams and three object beams, from which we get the three object beams ΣROD, ΣGOD and ΣBOD reconstructed by the holographic plate simultaneously with the three live object waves

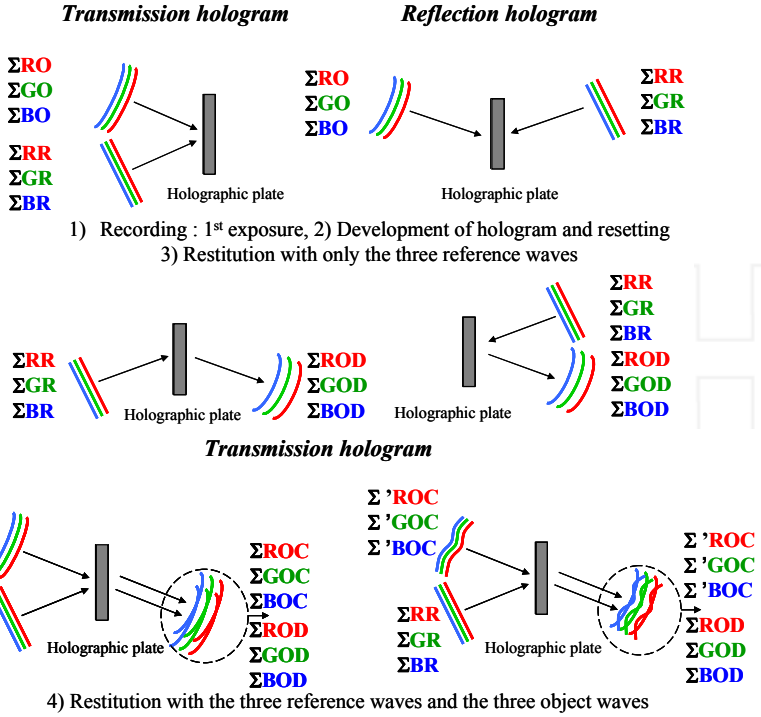

Fig. 2. Formation of colour interference fringes

transmitted ΣROC, ΣGOC and ΣBOC. The profiles of the ΣROD and ΣROC, ΣGOD and ΣGOC waves, and the ΣBOD and ΣBOC waves are strictly identical to each other if no change has occurred between the two exposures and if the hologram gelatine has not contracted during development. So there will be three simultaneous interferences among the object waves constructed by the hologram and the live object waves. In this case, a flat uniform colour can then be observed behind the hologram. If a change in optical path is created in the test section of wind tunnel, the three live waves will deform and adopt the profiles Σ'ROC, Σ'GOC and Σ'BOC while the waves reconstructed in the hologram, ΣROD, ΣGOD and ΣBOD, remain unchanged. Any colour variations representing optical path variations will thus be visualized in real time behind the hologram (Step 4, Fig. 2).

4. Real-time colour transmission holographic interferometry

4.1 Laboratory study of feasibility

4.1.1 Choice of laser and colour base

The following points have to be addressed to show the feasibility of real-time colour holographic interferometry. Firstly, a laser has to be found that will supply the three primary wavelengths forming as extensive as possible a base triangle[2]. It is an Innova

[2] The three wavelengths chosen define the three vertices of a triangle chromaticity diagram (MacAdam, 1985).

Spectrum 70 ionized gas laser (mixed argon and krypton) that produces approximately 10 visible lines with a total power of 4.7 W. The three wavelengths retained are 647 nm for the red line of krypton and 514 nm and 476 nm for the green and blue lines of argon. All three exhibit a TEM_{00} mode because thee laser is equipped with a Fabry-Perot etalon to increase the coherence length of the three lines selected. The etalon is treated on both faces to get 66% transmittance for the blue line, 63% for the green line and 61% for the red line. This treatment increases the blue line's coherence length 2 or 3 centimetres at a range of several tens of centimetres. This is sufficient because, in our study, the reference and measurement paths can be roughly equalized and the optical path variations to be measured are no greater than a few microns. In the other hand, a large light energy is needed to record the studied phenomena at ultra-high speed (35,000 f/s with an exposure time of 750 10^{-9} s).

4.1.2 Panchromatic holographic plates

Since Russian panchromatic plates came on the market twenty years ago, progress has been made in true colour holograms (Hubel, 1991; Bjelkhagen & Vukicevic, 1991; Bjelkhagen et al., 1996). The various chemical treatments applied to these plates are explained in detail by several authors (Bjelkhagen, 1993; Sasomov, 1999). The plates used are silver-coated single-film PFG 03C plates from the Slavich company in Moscow. Their chemical treatment first includes a hardening of the gelatine, development, bleaching, a series of rinses in alcohol and slow drying. The hologram's spectral characteristics were analyzed by taking a double exposure holographic interferogram and placing a small mirror near the object to be analyzed, in order to make a spectral analysis of the reconstructed light waves. The spectrograms of the reconstructed waves in our very first validation tests showed that the three peaks corresponding to the reconstructed colours are slightly shifted by a few nanometres, which corresponds to the contraction of the gelatine thickness:

- 471 nm for the blue, or $\Delta\lambda = -5$ nm,
- 511 nm for the green, or $\Delta\lambda = -3$ nm,
- 640 nm for the red, or $\Delta\lambda = -7$ nm.

These differences are reduced practically to zero in wind tunnel tests when the hologram is placed normal to the bisector of the angle formed by the object and reference beams.

4.1.3 Laboratory results

Fig. 3 shows the feasibility setup implemented in the laboratory. The Innova Spectrum laser emits eleven lines in the visible simultaneously. The red, green, and blue lines we want are diffracted by an acousto-optic cell in which are generated three frequencies f_1, f_2 and f_3 appropriate to the three wavelengths λ_1, λ_2 and λ_3. A beamsplitter cube splits the reference beams and three object beams. The three reference beams are collimated onto the holographic plate by an achromatic lens located a focal length from the pinhole (diameter 25 μm) of a spatial filter having a microscope objective lens (x60). The three object beams are collimated the same way to form three parallel light beams between two large achromatic lenses and illuminate the test section.

The hologram is thus illuminated on the same side by the three parallel reference beams and the three convergent measurement waves. A diaphragm is placed in the focal plane just in front of the camera in order to be able to filter out any parasitic interference. The hologram is first illuminated in the absence of flow and is then developed and placed back in exactly its original position. When the hologram is illuminated with the reference beam, nine diffraction images are seen. They are clearly visible in Fig. 4. Of the nine, three coincide and

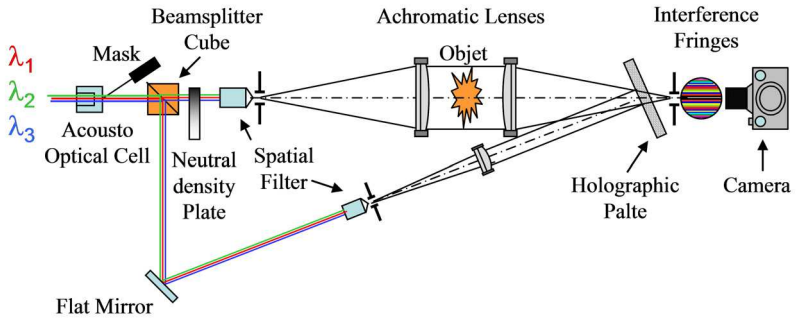

Fig. 3. Real-time colour holographic interferometry setup (Transmission mode)

focus exactly at a single point if the setup is perfectly achromatic. These three images correspond to the diffraction of the blue image by the blue beam, that of the green image by the green beam, and that of the red image by the red beam. They are exactly superimposed. The other six images are parasitic and have to be filtered out. They correspond to the diffraction of the blue image by the green and red lines, that of the green image by the blue and red lines, and that of the red image by the blue and green lines. Fig. 4 shows how all the images are diffracted behind the hologram, and the spatial filter system that is used to select only the focal point of interest to us.

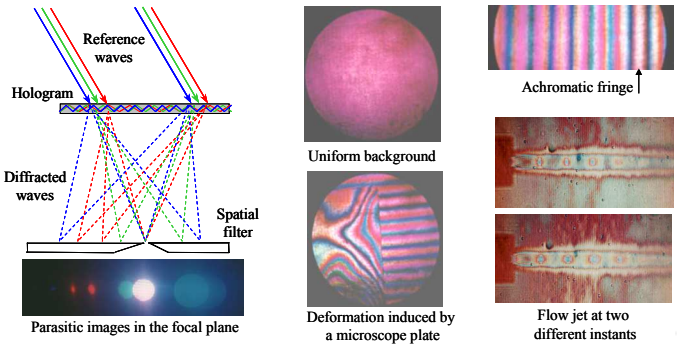

Fig. 4. Real-time colour holographic interferometry setup (Transmission mode)

Moreover, an adjustable neutral density filter made it possible to balance the power of the measurement beams with that of the reference beams. For reference, the power of the three lines at the acousto-optic output is 50 mW for the red line and 90 mW for the green and blue. In the hologram plane, the reference beam powers are 240 μW/cm² for the red line, 270 μW/cm² for the green, and 290 μW/cm² for the blue. For the object beams, one measured 100 μW/cm² for the red and green lines and 330 μW/cm² for the blue. The hologram exposure time for the first exposure was 4 s. Fig. 4 shows some images obtained. First, the uniform background colour was obtained over the entire surface of the test section, which shows that it is possible to re-position the three live waves simultaneously with the three waves contained in the hologram. The tint is the purple of the first order of interference, which is one of the most sensitive. The interference pattern is obtained by slightly displacing one of the two large achromatic lenses. So a horizontal, vertical, or even circular fringe

pattern can be formed. The achromatic central white fringe can be made out very clearly. One also can see the deformation due to an microscope plate and a small jet at two different instants. Lastly, the diffraction efficiency was measured behind the hologram. The hologram exhibits a diffraction efficiency of about 0.8% for the red and green lines and 0.5% for the blue line. Although these values are very low, they do allow a good visualization.

4.2 Wind tunnel adaptation of the method

The optical setup for testing the feasibility of the technique had to be modified and adapted around ONERA's wind tunnel at Lille centre. For reference, this wind tunnel is equipped with a 2D test section 200 mm high and 42 mm wide. The Mach number can be varied from 0.3 to 1.1. The flow studied was the unsteady flow downstream of a cylinder 20 mm in diameter D placed crosswise in the test section.

4.2.1 Optical setup around the wind tunnel

The optical setup is shown in Fig. 5. The beam power as it leaves the laser is 1.80 W when the etalon is set perpendicular to the laser beam axis and 1.20 W when it is tilted. The polarization of the three beams rotates 90° at the exit from the acousto-optic modulator, so that the polarization vectors lie parallel to the reflecting surfaces of the mirrors. This arrangement makes it possible to have beams of the same polarization interfere on the hologram. The three wavelengths downstream of the acousto-optic cell are split into a reference beam and object beam by a beam splitter cube. A right angle prism is used to adjust the reference and object path lengths on the hologram. A spatial filter is used to expand the beam for its passage through the test section. A pair of achromatic lenses converts the beam into parallel light in the test section and then focuses it on the hologram. The reference beam passes over the test section, and then another achromatic lens is used to illuminate the hologram with a parallel light beam. For reference, the object beam diameter is 40 mm at the hologram and that of the reference beam is 60 mm. At the acousto-optic cell, the power of the three light waves is practically the same (of the order of 70 mW per channel). The beam splitter cube distributes 85% of this power to the reference path and 15% to the measurement path.

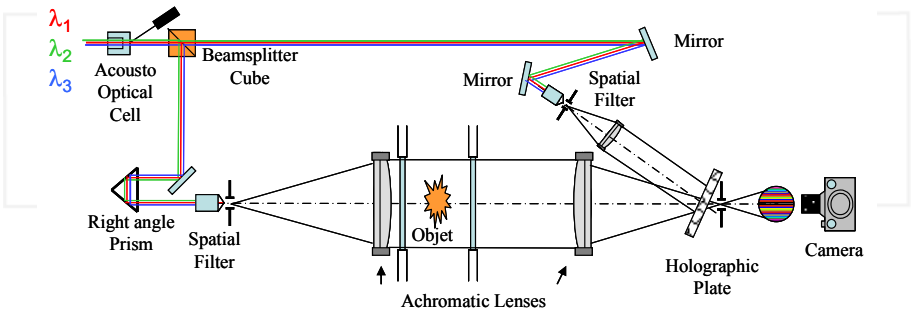

Fig. 5. Optical setup implemented around the wind tunnel

At the hologram, one measures 250 μW/cm² in the red and blue lines and 280 μW/cm² in the green line for the reference beam, while the object beam powers are 30 μW/cm² in the

red line and 40 μW/cm² in the green and blue lines. These proportions can be used to obtain a perfect balance among the powers of the three waves diffracted by the hologram when re-positioning it, and the three live waves. For reference, the hologram diffracts 70 μW/cm² in the red line, 65 μW/cm² in the green line, and 90 μW/cm² in the blue line. The first exposure lasts 2 s. The holograms are then subjected to treatments to harden the gel, develop it, and bleach it. When the hologram is put back in place, the light power at the camera entrance is 1.5 10^{-3} W at the focal point, which is sufficient to record interferograms at an ultra-high speed of 35,000 frames per second with an exposure time of 750 ns per shot.

4.2.2 Results and analysis of interferograms at Mach 0.37

Figure 6a gives a sequence of six interferograms of the flow around the cylinder at Mach 0.37. The time interval between each picture is 100 μs. One can see that each vortex is represented by concentric rings of different colours where each colour represents an isochoric line. The vortex formation and dissipation phases can be seen very clearly while the fringes oscillate between the upper and lower surfaces of the cylinder. Several types of measurements were made by analyzing a sequence of some 100 interferograms. First, the vortex centre defined by the centre of the concentric rings was located in space for each interferogram, which made it possible to determine the mean paths for the vortices issuing from the upper and lower surfaces. The results of this are shown in Fig. 6b. The "o" symbols represent the positions of the vortex centres from the upper surface, and the "•" symbols those of the lower surface. Remarkably, the two paths exhibit a horizontal symmetry about the x = 0 axis passing through the cylinder centre. One may also point out that even at x/D = 4 downstream of the cylinder, the upper and lower vortex paths do not come together and line up.

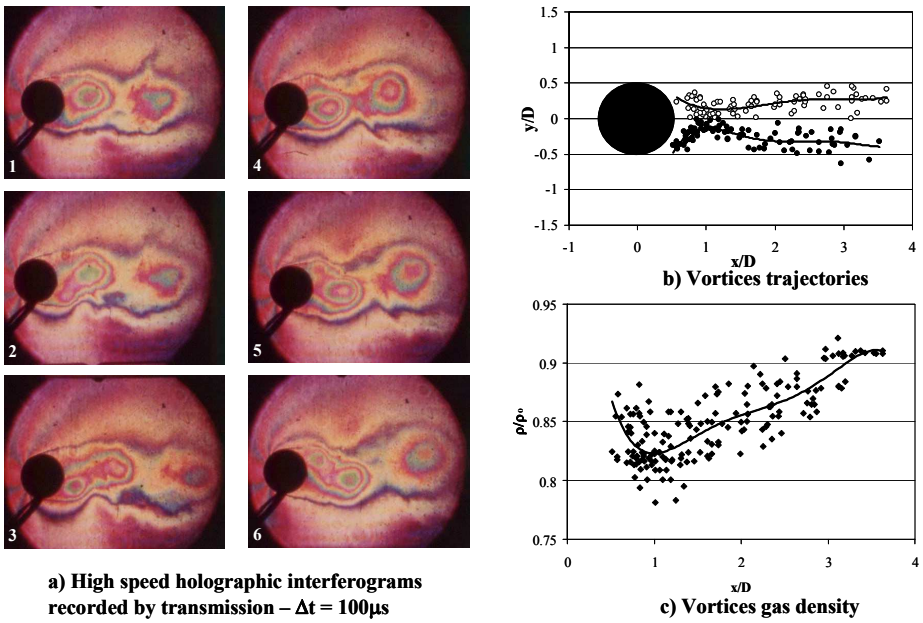

Fig. 6. Unsteady wake flow around the cylinder -Results and analysis – Mach 0.37

Lastly, the colours of each interferogram were analyzed using the "MIDI" software[3], which models the light intensity and experimental interference fringe colours as a function of the path difference (Desse, 1997a). The gas density measured under free stream conditions is the same as that measured at the outer flow of the wake (measured in the vicinity of the wind tunnel's upper and lower walls).
If e is the test section width and n the refractive index, the optical thickness E can be expressed by :

$$E = (n-1).e \tag{1}$$

Knowing the Gladstone-Dale relationship :

$$K = \frac{(n-1)}{\rho / \rho_s} \tag{2}$$

where ρ_s is the gas density under standard conditions (1.29 kg/m^3) and K the Gladstone-Dale constant (296.10^{-6}), the relative gas density variation is written :

$$\frac{\Delta\rho}{\rho_0} = \frac{\Delta E}{e.K}\frac{\rho_s}{\rho_0} \tag{3}$$

with $\Delta\rho = \rho - \rho_\infty$ and $\Delta E = E - E_\infty$, ρ_∞ being the gas density measured under free stream conditions and ρ_0 the stagnation gas density. Starting from a point external to the wake, one can work back to the gas density at the stagnation point (at the nose of cylinder) and measure the gas densities at the centre of the vortices. The graph of Fig. 6c shows how ρ/ρ_0 varies for the vortices emanating from the upper and lower surfaces. The trend curves plotted show the same variations. For $0.5 < x/D < 1$, the vortices are in a formation or agglomeration phase because the gas density decreases at their centre. Then, when $x/D > 1$, the vortices enter a dissipation phase because the gas density increases again at their centres. The drop in gas density is large, reaching about 20% ρ_0. A rather large dispersion may nonetheless be noticed in the data. This is due mainly to our determination of the vortex centre locations, which are not very easy to determine when the vortices are in the dissipation phase. Moreover, taking the hologram transfer function into account in the exact modelling of the interference fringes should greatly improve the modelled colours between the orders of interference, and thereby the measurement precision.

5. Real-time colour reflection holographic interferometry

Since transmission holograms are used, the diffraction efficiency of holograms just reaches between 10% and 20%, which limits the quality and the contrast of interferences fringes. On the other hand, if reflection holograms are used, the theoretical diffraction efficiency can reach 100% with a monochromatic light. The development of real-time true colour reflection holographic interferometry also offers two important advantages. The first one concerns the analysis of the three-dimensional (3D) flows and the second one lies in the comparison with digital colour holographic interferometry. In fact, ONERA is looking towards analyzing unsteady 3D flows, and the optical setup to be designed must be based on several crossings

[3] Modelling of Luminous Interferences and Analysis of Interferograms

of the flow along different view angles. It is very evident that classical optical setup based on monochromatic holographic interferometry defined in section 4, for instance, for analyzing two-dimensional (2D) flows, cannot be reproduced three or four times. Moreover, as the optical path differences to be measured are smaller in 3D flows than in the 2D case, it is preferable that each optical ray crosses the phenomena twice in order to increase the sensitivity. Also, to simplify the setup, all the optical pieces have to be located on the same side of the wind tunnel, except the flat mirror which reflects the light rays back into the test section.

In literature, several authors have analyzed 3D flows using multidirectional tomography (Cha & Cha, 1996; Yan & Cha, 1998). They present holographic interferometric tomography for limited data reconstruction to measure an asymmetric temperature field. Other researchers designed an optical scheme for obtaining specklegrams simultaneously in four directions (Fomin, 1998; Fomin et al., 2002) or built an interferometric tomography apparatus with six viewing directions from which multidirectional data sets were analyzed following a method of examining spatial coherence (Pellicia-Kraft & Watt, 2000, 2001). The same approach is used by researchers developing digital holographic interferometric techniques. Timmerman & Watt (1995) developed a dual-reference beam holographic interferometer providing six simultaneous views of a compressible flow. One can also note the optical tomograh using six views interferometers for the measurement of 3-dimensional distribution of temperature in an evaporating liquid (Joannes et al, 2000). All the measurement techniques yield either the derivative of the refractive index (speckle holography, differential interferometry or back oriented schlieren) or the refractive index itself (holographic interferometry) and, very often, the spatial resolution of recording camera is very low compared to that of a holographic plate. As the reconstructed field depends strongly on the measured quantity, on the number of the viewing directions and on the spatial resolution, ONERA wanted to develop a metrological tool having limited viewing directions (three or four), high spatial resolution and yielding absolute value of the gas density in the field.

In colour holographic image and panchromatic holographic materials, one can note the recent work of Bjelkhagen & Mirlis, 2008 who produce highly realistic three-dimensional images. They show that the quality of a colour hologram depends on the properties of the recording material and the demand on a panchromatic material for colour holography is described.

5.1 Description of optical bench

The optical setup could be named “Denisyuk” because it uses a holographic plate in a classical Lippmann-Denisyuk in-line experiment. To obtain a very simple setup, all the optical pieces are located on the same side of the wind tunnel, except the flat mirror which reflects the light rays back into the test section. Due to these considerations, the optical setup based on real-time colour reflection holographic interferometry has been designed. It is presented in Fig. 7.

Here, the light source used behind the interferometer is constituted with three different lasers. An argon-krypton laser delivers the red line (λ_1 = 647 nm), and a green line (λ_2 = 532 nm) and a blue line (λ_3 = 457 nm) are given by two diode pumped solid state lasers. A spatial filter SP is just located at the focal point of the large achromatic lens AL3 (see photograph, Fig. 7) which is set in the front of the test section TS so that the object under

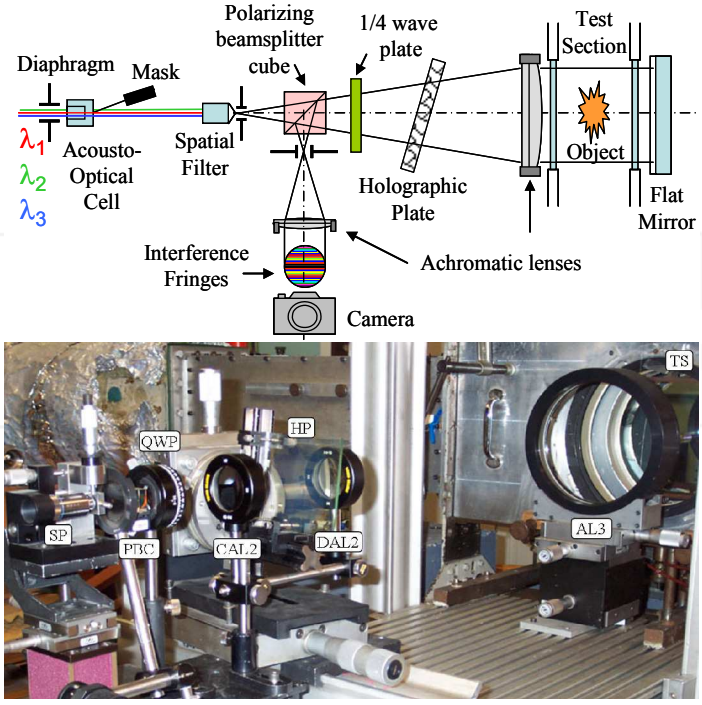

Fig. 7. Real-time three-color reflection holographic interferometer

analysis is crossed by a parallel light beam of 200 mm in diameter. A flat mirror located just behind the test section returns the three beams on the hologram HP inserted between the quarter wave plate QWP and the large achromatic lens. The hologram is illuminated on the two sides by the three collimated reference and measurement waves which are formed by the convergent and divergent achromatic CAL2 and DAL2 lenses (not shown in scheme of Fig.7). This arrangement allows one to easily obtain before the test a uniform background colour (infinite fringes) or narrowed fringes (finite fringes). In this setup, a polarizing beam splitter cube PBC is inserted between the spatial filter and the quarter wave plate which transforms the waves polarization twice (from P parallel to circular and from circular to S parallel) so that, when the rays are returning, the beam splitter cube returns the rays towards the camera. A diaphragm is placed in the focal plane just in front of the camera in order to filter out any parasitic interference. The interferences fringes produced by the phenomenon under analysis can be directly recorded using high speed camera. Here, the camera used is a CORDIN 350 Dynafax. The size of each recording is 10x8 mm² and the pictures are taken in a staggered pattern on a 35mm film. High sensitivity (800/1600 ASA) daylight reversible colour films are suitable.

5.2 Principle of real-time three-color in-line holographic interferometry

Fig. 8 details how the interferences fringes are generated in the real-time three-color reflection holographic interferometer.

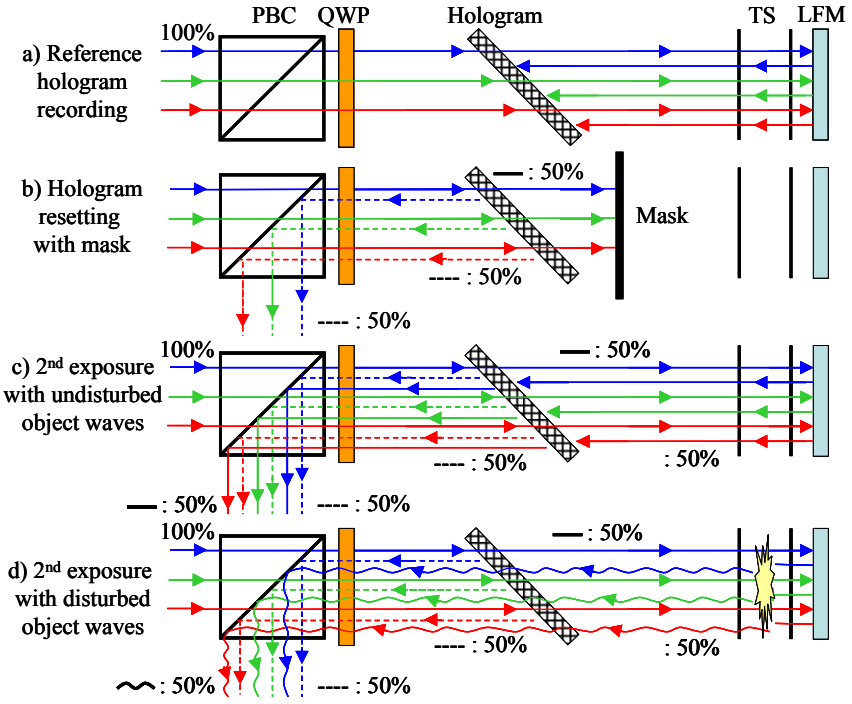

Fig. 8. Formation of colour interference fringes in optical setup

First, the holographic plate HP is simultaneously illuminated with the three wavelengths (Fig. 8a). The panchromatic hologram records simultaneously the three sets of interference fringes produced by the three incident waves and the three waves reflected by the flat mirror LFM (first exposure). Then the hologram is developed and it is reset in the optical bench at the same location. At the second exposure, if the diffraction efficiency of the holographic plate is near to 50% for the three lines, 50% of the light is reflected by the hologram (dashed lines) and 50% crosses the holographic plate (solid lines). If a mask is inserted in the front of the test section, one can observe on the screen the three images diffracted by the plate (Fig. 8b). This operation allows for verifying the quality of the holograms diffracted. When the mask is moved, 50% of the light crosses the test section twice and interferes in real-time with the three references waves (solid lines). Interference fringes are not localized because they can be observed from the holographic plate to the camera. If no disturbances exist in the test section, a uniform background colour is obtained in the camera (Fig. 8c). If variation in refractive index exists in the test section, colour fringes will be seen on the screen. As the luminous intensities of reference and measurement waves are basically equal, the contrast of colour interferences fringes will be maximum (Fig. 8d).
This optical setup is very simple but it presents some advantage and some inconvenience. The advantage lies in the small number of optical pieces which are used. The reference beams and the measurement beams are co-linear and there is just a flat mirror behind the test section. The contrast of colour interferences fringes depends on the diffraction efficiency of the holographic plate and the colours saturation depends on the luminous intensity of the

three wavelengths which can be adjusted with the acousto-optic cell. A main inconvenience resides in the fact that it is not possible to adjust the diffraction efficiency of the holographic plate. It is only fixed by the chemical treatment and it is a function of gelatine thickness. The unique solution to solve this problem will consist in a specific treatment of the surface of the flat mirror and this operation implies prior knowledge of the diffraction efficiency of the hologram.
Finally, the three interference fringe patterns will exist and can be recorded if the coherence length of the three wavelengths is more than twice the distance between the holographic plate and the flat mirror located just behind the test section. Compared to the setup of transmission holographic interferometry, here it is not possible to adjust the length between the reference and measurement rays. In this experiment, two types of holographic plates have been tested: Russian plates (PFG03C) from Slavich and French plates (Ultimate 08) from Gentet, typically 10 μm thick. For information, energies at each wavelength applied at the first exposure are given in Table 1 for Slavich and Gentet plates.

PFG03c (Slavich)	Ultimate 08 (Gentet)
1.0 10^{-3} J/cm² @ 457nm	0.8 10^{-3} J/cm² @ 457nm
1.3 10^{-3} J/cm² @ 532nm	0.8 10^{-3} J/cm² @ 532nm
1.0 10^{-3} J/cm² @ 647nm	0.8 10^{-3} J/cm² @ 647nm

These values can be compared with tests and results found in Petrova et al., 2000 who determine the holographic characteristics of panchromatic light sensitive material for reflective 3D display.

5.3 Problem of gelatine shrinkage

The problem of gelatine shrinkage is described in detail in Desse, 2006. In Fig. 9, one can see how the interference fringes are inscribed into the gelatine when the holographic image is recorded by transmission or reflection. In transmission, the interference fringes are perpendicular to the plate and a small variation in the gelatine thickness caused by the chemical treatment of the hologram does not modify the three inter fringe distances. On the other hand, in reflection, interference fringes are recorded parallel to the plate surface and the inter fringe distance is very sensitive to a small variation of the gelatine thickness. Fig. 9 presents the effects of the gelatine contraction when a reflection hologram is recorded with a green wavelength (514 nm). At reconstruction, a white light source (xenon source) illuminates three different holograms at the incidence angle that the reference wave had at recording. One can see that if the gelatine thickness is kept constant (Δe=0), the hologram only diffracts the recording wavelength, i.e. for the green hologram, the green wavelength contained in the xenon spectrum. If the gelatine thickness has decreased by 5%, (Δe = -0.5 μm), the fringe spacing will be proportionally reduced and the diffracted wavelength will be shifted by a quantity equal to

$$\Delta\lambda = \frac{\lambda}{e}\Delta e \tag{4}$$

where e is the gelatine layer thickness (about 10 μm). The hologram will diffract a wavelength equal to 488.3 nm corresponding to a blue line and, if the gelatine thickness increases by 10% (Δe>0), the hologram illuminated in white light will diffract a wavelength close to yellow (565.4 nm).

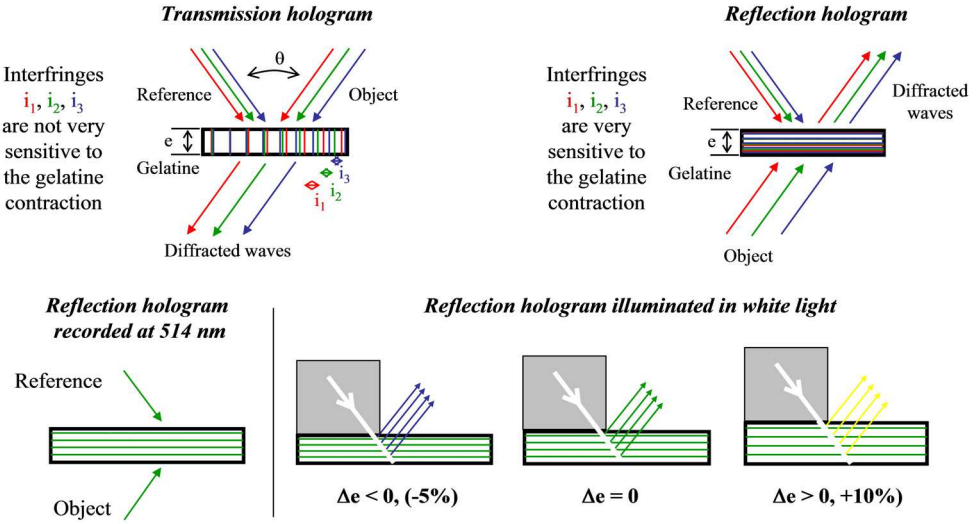

Fig. 9. Effect of the gelatine contraction on the different waves

On the other hand, it is well known that the chromatic perceptibility of eye δl varies with the wavelength. It is defined as being the variation δl between two different wavelengths perceived by the eye at constant luminosity. It is about 1 nm in the green and yellow colours and 6 nm in the blue and red colours, which corresponds to relative variations of 0.2% and 1.5% respectively. For the diffracted colour change not to be detected by a human eye, it is mandatory that $\delta l/\lambda$ has to be less than $\delta\lambda/\lambda$ that which implies that the variation in gelatine thickness should be less than 0.2%. This means changes in thickness of more than 20 nm are not acceptable. As the optical technique is based on the knowledge of the true colours diffracted by the hologram, variations of the gelatine thickness are a cause of large errors in the data analysis. It is for this reason that the gelatine shrinkage problem has to be perfectly mastered.

5.4 Gelatine contraction control

In this experiment, two types of holograms have been tested: Russian plates from Slavich and French plates from Gentet. Concerning the first ones, a specific treatment proposed by Kim, 2002, has allowed obtaining a gelatine contraction smaller than 20 nm by mixing 2 ml of glycerol in the last bath of ethanol (100% ethanol drying). One can mention that the treatment applied to the Russian plates includes about ten steps and it is very sensitive to the temperature and the PH of the solutions. About the French plates, following Gentet's recommendations, we have also obtained basically no variation in the gelatine thickness diffracted by Gentet and Slavich plates when they are illuminated in white light.

In these graphs of Fig. 10, the dashed lines represent the spectrum of white light diffracted by the holograms with no treatment of the plates. We can observe a shifting of about 1.8 % with Gentet holograms and about 1.1% with Slavich holograms which is not acceptable. It can be also seen that the spectrum diffracted by Gentet holograms is wider than the spectrum diffracted by Slavich holograms. For example, if one looks at the red line at a

normalized intensity of 0.4, the width of the curve is near to 16 nm and 27 nm for the Slavich and Gentet holograms respectively. It is of 10 nm and 17 nm for the blue line. If a small variation of the gelatine thickness is allowed then the wider spectral response of Gentet holograms is advantageous. A bad adjustment of the Fabry-Perot etalon in the argon-krypton laser cavity, meaning that the coherence length was reduced, explains the weakness of the green response in the Slavich graph.

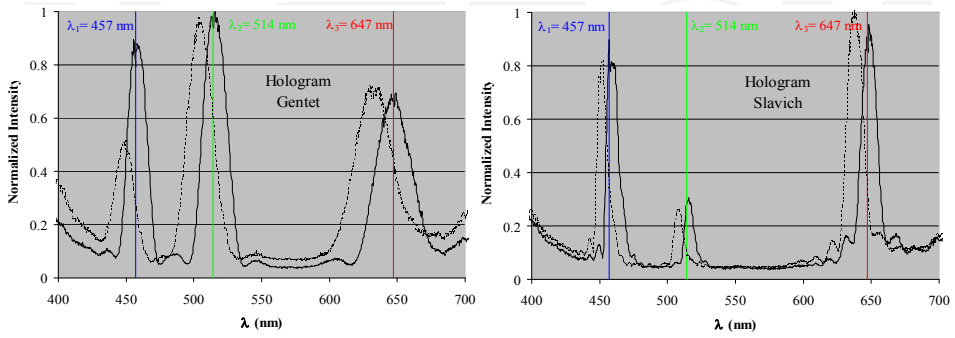

Fig. 10. Measurement of the gelatine shrinkage – Gentet and Slavich holograms

When no shrinkage exists, the curves are basically centred on the three different lines of the lasers and the best diffraction efficiency of hologram is reached. The three different gratings inscribed in the hologram gelatine diffract very well the three different wavelengths (blue, green and red) of the laser sources. In fact, the response of the hologram is the best one because the bell curves are centred on the three laser wavelengths. In these conditions, there is basically no difference in the gelatine thickness before and after the chemical treatment of the plates. Moreover, if the power of the three reference and measurement wavelengths are the same, it is possible to obtain very bright, high contrast fringes.

5.5 Diffraction efficiency measurement

The diffraction efficiency DE of the holographic plates can be evaluated when Russian or French plates are illuminated in white light. For example, Fig. 11 shows how the diffraction efficiency of Gentet holographic plate is determined from the spectrum of the xenon light source transmitted by the plates. It very easy to see the three hollows corresponding to the part of the white light diffracted by the Gentet holographic plate. For each line, the bandwidth can be determined when the diffraction efficiency is more than 35%. In fact, as regards luminous intensity, when the diffraction efficiency of the holographic plate is equal to or more than 35%, the visibility coefficient of interference fringes $((I_{max}-I_{min})/(I_{max}+I_{min}))$ is near to 0.21, that means the colour interference pattern will be of very high? contrast. For the blue line, the acceptable wavelength shift is 8 nm (1.75%), 9 nm (1.75%) for the green line and 13 nm (2%) for the red line. This particularity is very interesting because the theoretical constraints on the variation of the gelatine thickness (near 0.2%) become larger (about 1.75%) due to the spectral broadening of the transmission curve.

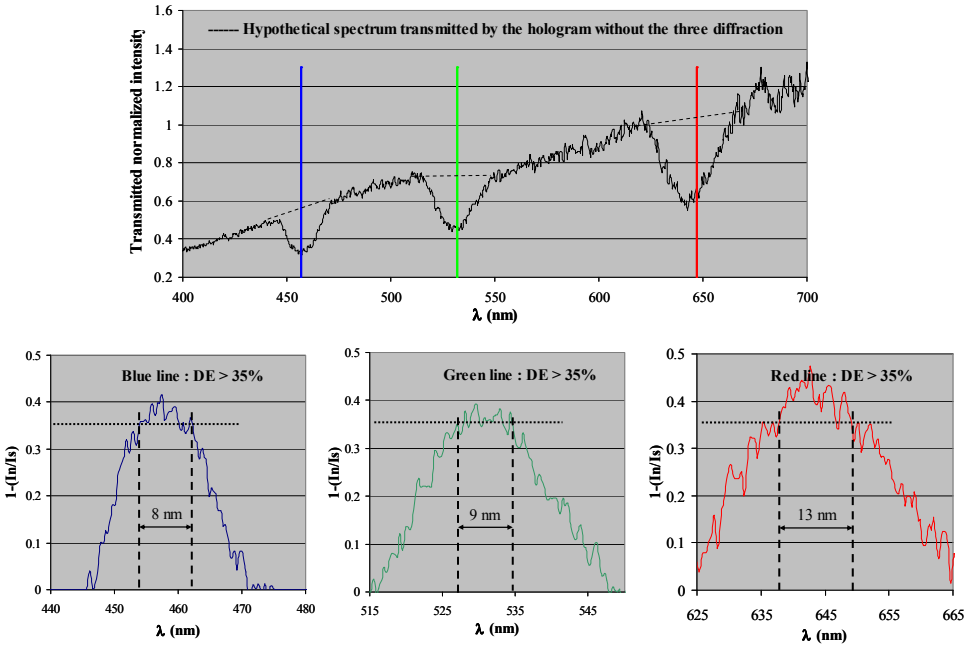

Fig. 11. Evaluation of diffraction efficiency of Gentet plate

5.6 Wind tunnel implementation of optical technique

A real-time colour reflection holographic interferometer has been implemented in the ONERA transonic wind tunnel for analyzing the same unsteady wake flow around the cylinder. In this experiment, the infinite Mach number was fixed at 0.45 and the high speed interferograms were recorded with the rotating drum camera which is equipped with a 400 ASA colour film. The time interval between two successive frames is 117 μs. The time exposure (750 ns) of each interferogram is given by a small window size inside the camera and the number of recorded interferograms is about 220. The images are 8x10mm² in size and they are digitalized with a SONY 325P video camera through a Matrox image processing board. Several movies have been recorded with uniform background colour (infinite fringes), circular and narrowed fringes (finite fringes). As the optical setup is very sensitive to external vibrations, the uniform background colour is difficult to adjust when the wind tunnel is running, but the fringe formation can be observed on the hologram surface so that it is possible to adjust the uniform background colour with the wind tunnel operating. Fig. 12 shows three of twelve interferograms covering about a period of the vortex street. They are recorded in infinite fringes. The interferogram colours are well saturated and of higher contrast than those obtained in previous experiments performed with transmission holograms (see interferograms of Fig. 6).

When the background colour is uniform, it is very easy to follow the vortices emitted from the upper and lower side. For instance, if one looks at the colours coming out in the vortex cores, one can easily see that the first vortex emitted from the upper side enters a formation phase where the gas density decreases in the vortex centre. A second phase of dissipation is

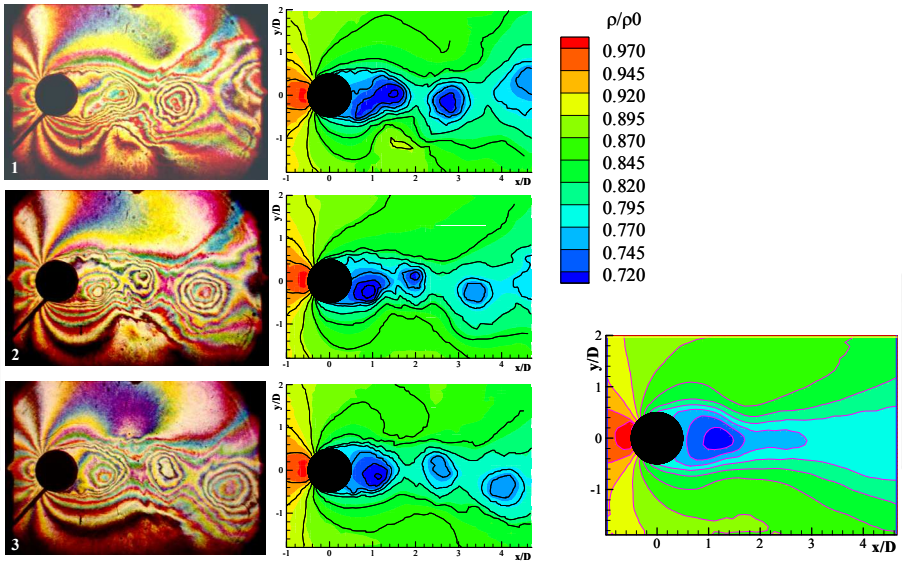

Fig. 12. Interferogram analysis : instantaneous and average gas density field – Δt = 117µs

observed looking at the last vortex leaving the observed field. Finally, as with transmission holographic interferometry, each colour represents a value of the gas density. In analysis, the gas density field was referred to ρ_0, the stagnation gas density. One can see that the instantaneous gas density varies from 0.70 to 0.98. The average gas density in the field has been calculated from twelve successive interferograms. The interferogram number is not very significant, but the obtained field is already symmetrical enough and the gas density varies from 0.72 to 0.97. Finally, if the colour scale of interference pattern is very well known to the user, the image of interferograms is sufficient to correctly evaluate the evolution of the gas density field.

6. Digital colour holographic interferometry

The fast development of technology, such as high resolution sensors, various DPSS lasers with large coherence, data post processing and computation power provide now opportunities to conceive new optical methods capable of simultaneous full field measurements with high spatial and temporal resolutions and giving absolute data. Digital holography with matrix sensors appeared in the last decade with cheap high resolution CCD cameras and the increasing power of computers. Image sensors have now size and spatial resolutions compatible with the needs for digital holographic recording. For example, matrices with 1636×1238 pixels of size 3.9×3.9µm² are now available (Yamaguchi & Zhang, 1997). In the literature, only few papers concern works in digital colour holographic interferometry. In 2002, Yamaguchi et al. & Kato et al. demonstrated phase shifting digital colour holography using a multi-wavelength HeCd continuous wave laser (636nm, 537.8nm, 441.6nm) and a colour CCD equipped with a Bayer mosaic[4]. The authors demonstrated the

[4] Matrix structure in front of a sensor to create a colour information from a panchromatic monochrome

possibility for the reconstruction of colour images but experimental results have a relatively low spatial resolution since the effective pixel number at each wavelength was 818×619, leading to an effective pixel pitch of 7.8μm. Demoli et al., 2003, presented the first study on fluids using digital colour Fourier holography. They used a monochrome CCD sensor and three wavelengths from three continuous wave lasers (647nm, 532nm, 476nm). Their results show the evolution of thermal dissipation in an oil tanker with an excellent resolution, by using the amplitude image of the reconstructed holograms. Note that historically the use of several wavelengths for holographic interferometry was first described by Jeong et al., 1997. Furthermore Ecole Popytechnique Fédérale de Lausanne's researchers (Kuhn et al., 2007) and INOA (Ferraro et al., 2007) proposed the use of several wavelengths in digital holographic microscopy. For quantitative phase microscopy, Ferraro et al., 2004, showed that severe chromatic aberration can be eliminated. Since the main effect of the chromatic aberration is to shift the correct focal image plane differently at each wavelength, this can be readily compensated by adjusting the corresponding reconstruction distance for each wavelength. In these works the recording at each wavelength is sequential. Such approach was applied in three dimensional image fusion using sequential colour recording at several distances (Javidi et al., 2005). Such strategy was also considered by J. Zhao et al., 2008, by using three laser wavelengths as an imaging approach. All these methods use sequential recording at each wavelength and generally off axis reference waves are incident on the recording area at a constant angle. At the same time, two wavelength profilometry was proposed in a digital holographic microscope using two laser diodes (680nm, 760nm) and a monochrome sensor, giving a synthetic wavelength of 6.428μm (Kuhn et al., 2007). The method is based on a spatial multiplexing by incoherent addition of single-wavelength interferograms, in the same way as was developed by Picart et al., 2003, 2005, with a single wavelength, each having different propagation directions for the reference waves, and recording with a monochrome CCD.
As regards these works, ONERA and LAUM[5] decided to join theirs respective competences acquired in the past in order to develop adaptable and new optical imaging methods, firstly having properties such as full field imaging with high spatial and temporal resolutions, secondly giving absolute data after post processing and finally giving dynamic three dimensional measurements. These non-invasive optical methods are based on digital colour holography.

6.1 Theoretical basics

In the case of Fluids Mechanics, hologram analysis performed by direct and inverse two-dimensional FFT algorithms is very well adapted for the reconstruction of transparent phase objects. For any wavelength λ, the recorded image plane hologram can be expressed as:

$$H_\lambda(x,y) = O_0(x,y) + R(x,y)O^*(x,y) + R^*(x,y)O(x,y) \tag{5}$$

where $O_0(x,y)$ and $R(x,y)$ are the zero order and the reference wave respectively and $O = b_\lambda exp(i\varphi_\lambda)$ is the object wave. For convenience, $R(x,y)$ can be represented with unit amplitude and zero phase. Subscript λ refers to one of the three colours, that is $\lambda = R, G$ *or* B. In the case of in-line holography, computation of the Fourier transform gives a broad spectrum centred at the zero spatial frequency. So, no relevant information can be extracted from such a spectrum. Consider now off-axis holography in which a spatial carrier is introduced along x

[5] **L**aboratoire d'**A**coustique de l'**U**niversité du **M**aine, Prof. P. Picart, Le Mans, France

or y or along the two directions. In a general case, $2\pi(u_\lambda x+v_\lambda y)$ is the spatial carrier modulation along xy, the hologram becomes:

$$H_\lambda(x,y)=O_0(x,y)+O(x,y)\exp\left[2i\pi\left(u_\lambda x+v_\lambda y\right)\right]+O^*(x,y)\exp\left[-2i\pi\left(u_\lambda x+v_\lambda y\right)\right] \quad (6)$$

By developing complex exponentials one obtains:

$$\begin{aligned} H_\lambda(x,y)=O_0(x,y)+b_\lambda(x,y)\exp\left[i\varphi_\lambda(x,y)\right]\exp\left[2i\pi\left(u_\lambda x+v_\lambda y\right)\right] \\ +b_\lambda(x,y)\exp\left[-i\varphi_\lambda(x,y)\right]\exp\left[-2i\pi\left(u_\lambda x+v_\lambda y\right)\right] \end{aligned} \quad (7)$$

Fourier transform of Eq. (7) gives:

$$\tilde{H}_\lambda(u,v)=A_\lambda(u,v)+C_\lambda(u-u_\lambda,v-v_\lambda)+C_\lambda^*(u+u_\lambda,v+v_\lambda) \quad (8)$$

where $C_\lambda(u,v)$ and $A_\lambda(u,v)$ are respectively the Fourier transform of $b_\lambda(x,y)exp[i\varphi_\lambda(x,y)]$ and $O_0(x,y)$. If the spatial frequencies u_λ and v_λ are well chosen, the three orders are well separated in the Fourier plane. Applying a binary mask around the frequency $+u_\lambda$, $+v_\lambda$, respectively of width Δu and Δv, allows the extraction of the object optical phase $\varphi_\lambda(x,y)$. Inverse Fourier transform applied to the selected region gives an estimation of the object complex amplitude and of the impulse response corresponding to the filtering applied in the Fourier domain (Desse et al., 2008).

This is quite easy to do if the hologram is not too noisy or if the optical phase $\varphi\lambda$ has a narrow spectrum. Practically, the spectral lobe of the first order diffraction can be manually selected in order to make it more reliable. When the test object is modified, for instance by a flow, this induces a modification in the refractive index along the probe beam and thus this modifies the optical path and then the optical phase. At any wavelength λ, recording a new hologram $H_\lambda(x,y)$ leads to the computation of phase. The phase change between the two states of the object is simply obtained by computing. In a setup where the test section is crossed twice, the optical path difference due to the phenomena is given by:

$$\delta=\frac{\lambda}{4\pi}\Delta\varphi_\lambda \quad (9)$$

6.2 Digital Michelson holographic interferometer

The assembly shown in Fig. 13a is very simple. It is like a conventional Michelson interferometer in which a beamsplitter cube is inserted between the spatial filter and the test section. The spatial filter is placed at the focal point of the achromatic lens so that the test section is illuminated with a parallel light beam as in previous optical setups. 50% of the light is reflected from the concave spherical mirror to form the three reference beams and 50% of light passes through the test section to form the three measurement waves. The flat mirror, placed just behind the test section, returns the beams towards the beam splitter. 25% of light is focused on the diaphragm which is placed in front of the camera lens. So, 25% of the reference beam intensities are focused in the same diaphragm by the concave mirror.

The generation of micro-fringes used as spatial carrier frequencies is shown in Fig.14. When the focal points of the reference and object waves are superimposed in the diaphragm which is placed in front of the camera, a uniform background colour is observed on the screen. If the focusing point of reference waves is moved in the plane of the diaphragm, straight

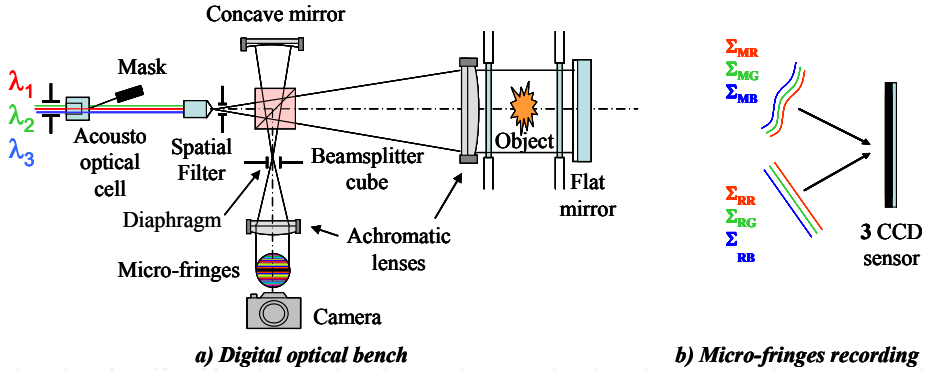

Fig. 13. Digital colour holographic interferometer – Formation of spatial carrier frequencies

interference fringes are introduced into the field of visualization. These micro fringes are recorded on the CCD in order to calculate the three reference phase maps. Then the wind tunnel is started and the three object waves are distorted by the aerodynamic phenomenon. Micro-fringes interference is again recorded by the 3CCD sensor to enable calculation of the phase maps related to the object. For maps of phase difference, the reference phase is subtracted from the phase object.

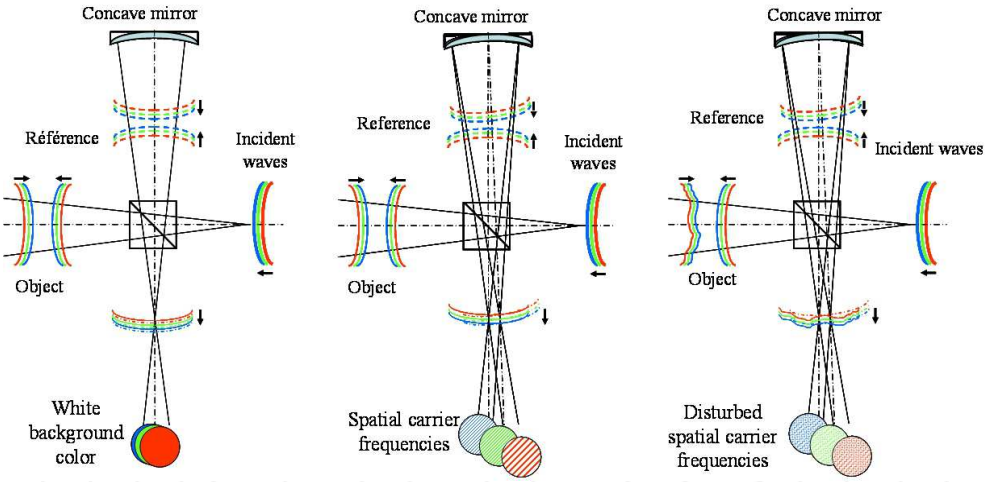

Fig. 14. Generation and micro-fringes formation by the phenomenon studied

6.3 Results obtained in subsonic wake flows

Again, near wake flow downstream from a circular cylinder has been studied at Mach 0.45. Here, one used a ORCA-3CCD Hamamatsu camera with 3 chips of 1344x1024 pixels, 6.45 µm x 6.45 µm in size. The framing rate is 9 f/s and the filters of RGB camera are very narrowband and centred on the three laser wavelengths. As the framing rate is very slow compared to the frequency of the vortex street, a transducer has been implemented in the cylinder at an azimuth of 90° (perpendicular to the flow axis) in order to synchronize the

interferogram recording with the signal of the unsteady pressure measurement. The cycle of the vortex street was decomposed in eight different instants shifted by 76 μs and at each instant, five interferograms were recorded from several cycles to average the unsteady maps. First, Fig. 15 shows two micro fringes images recorded with and without the flow in order to constitute reference and object interferograms. It can be seen in the zoomed image that micro-fringes are deformed by the shear layer of the upper side.

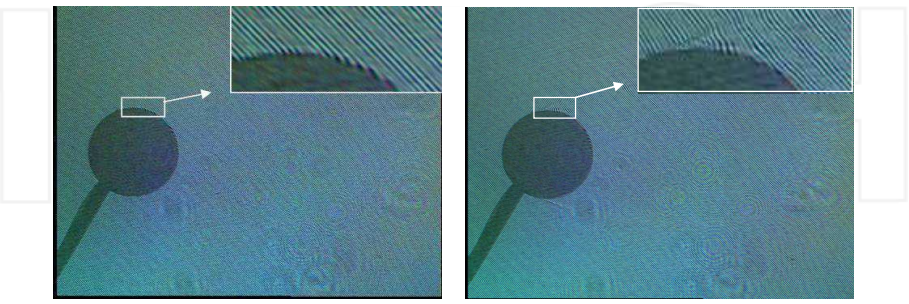

Fig. 15. Micro-fringes recording for the reference and object images

The three Fourier transforms are calculated from each image in order to reconstruct the phase maps with the +1 order (the zero order and the -1 order are filtered). An example of reference and measurement spectra is given in Fig. 16 for the green line. One can see that the spectrum only exhibits a spot corresponding to the green spatial carrier frequency. No parasitic frequencies due to the blue and red lines are found. By subtracting the reference phase maps from the measurement phase maps, one obtains the modulo2π phase difference maps. After unwrapping, it possible to compute the refractive index maps and the gas density field assuming the Gladstone-Dale relation.

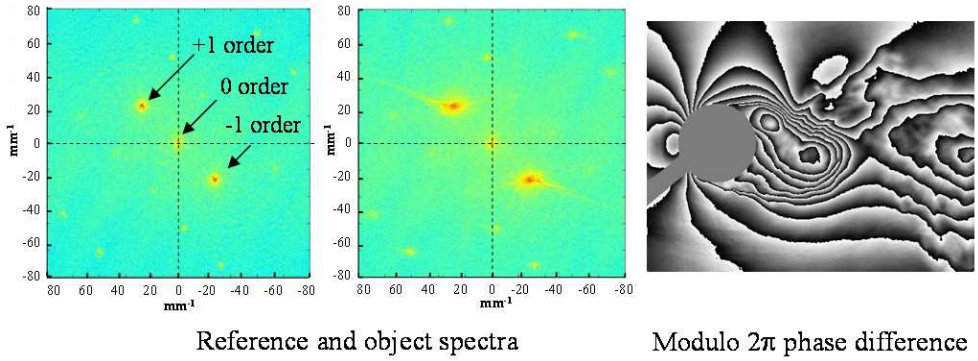

Fig. 16. FFT reference and object spectra and difference phase map for the green line

Colour interferences fringes and gas density field are shown in Fig. 17 for the first three images of one cycle of the vortex street.

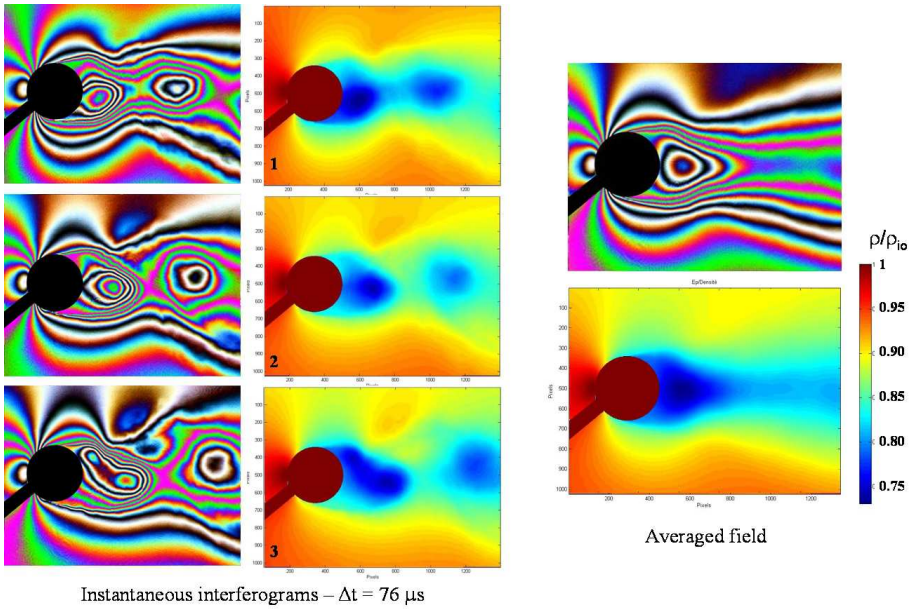

Fig. 17. Evolution of colour interference fringes and gas density field – Mach 0.45

The intensity of the interference fringes is computed on the three channels R, G, B from the phase maps with following the following relationship :

$$I_\lambda = A_\lambda(1 + \cos(\Delta\phi_\lambda)) \tag{10}$$

The gas density measured to the cylinder nose is particular as the gas density is equal to the stagnation gas density though the position of the vortex street, that means the colour found at this point has to be the same on each interferogram. Here, the intensity of colour interferences fringes is computed by imposing the white colour (δ = 0 µm) on each interferogram. Note this shifting is only made possible by the use of colour in the experiments. The time evolution of the gas density fields shows that the gas density decreases to 73% of ρ_{io} in the vortex core. Then, the averaged field of one cycle is calculated by averaging the 8 maps of instantaneous gas density field.

6.4 Comparison between holographic plate and digital holograms

As regards previous results obtained, silver-halide plate and digital holographic interferometry can be compared. The only possibility to compare plate and digital interferograms is to compare the interferograms displaying the interference fringes. Indeed, the technique of holographic interferometry in real time using panchromatic plates directly displays the colour density variations of the flow. It's a light intensity information that is obtained. With digital holography, the three monochromatic intensity maps are superimposed to obtain a colour map of the intensity of the interference fringes. This map

can then be compared to that obtained using the reflection holographic plates. After locating an interferogram recorded at a phase very similar to that of digital interferogram, Fig. 18 shows that the correspondence is very good.

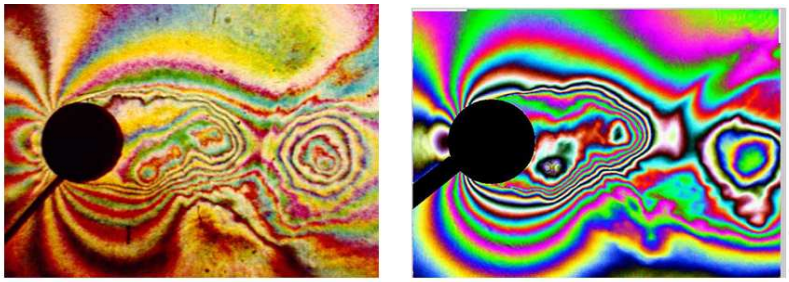

Fig. 18. Comparison between image and digital interferogram

So, in image colour holographic interferometry, a reflection panchromatic holographic plate (7,000 to 10,000 lines per mm in spatial resolution) has to be illuminated with a total energy of 600 μJ and the resetting of holographic plate is very sensitive and delicate. In digital technique, energy of 1μJ is sufficient to illuminate the sensor (155 lines per mm in resolution). The implementation is easy enough and the phase difference is entirely estimated with a computer. The coherence lengths of the three lasers must be more 2 meters in the two optical setups. In image holographic interferometry, about 220 successive frames of the phenomenon can be recorded at high framing rate (35,000 images per second with an exposure time of 750 ns for each). Each image has to be digitalized and processed. Also, it is important to obtain a reference hologram of about 50% diffraction efficiency for the three lines. In digital holographic interferometry, the framing rate is limited to 9 frames per second, full size and a synchronized triggering of interferograms recording has to be used to analyze unsteady phenomena.

7. Conclusion

The possibilities of image and digital colour holographic interferometry have been demonstrated. Colour holographic interferometry using panchromatic plates will continue to be used due to the high resolution of holographic plates. In near future, digital three-wavelength holographic interferometry seems the best candidate to characterize the future complex flows. Although CCD resolution and size are not as good as that of holographic plates, the digital approach is more accessible and versatile since the time for the hologram processing is greatly reduced and the processing is purely numerical. On the other hand, the value of using colour has been demonstrated as the zero order fringe can be easily determined and the variation in the background colour due to disturbances can be quantified. The limitations of the digital method seem to lie in the wide spectral sensitivity of the sensor which produces light diffusion in each monochromatic hologram. Work is currently in progress for removing the colour diffusion using a segmentation approach. Success in this strategy will allow increasing the spatial resolution in the reconstructed object. Future work will focus on the extension of the proposed technique for analyzing 3D

unsteady wake flows. At present, a specific setup of digital holographic interferometry has been defined in a single sight direction, and the aim will be to reproduce the same optical setup along several sight directions, each shifted by a given angle. It is obvious that the optical setup can be reproduced no more than three or four times. But the lack of sight directions should be compensated by high tomographic interferogram resolution for the reconstruction of the 3D gas density field.

8. Acknowledgments

The author thanks Jean-Louis Tribillon, retired, from Délégation Générale à l'Armement and Félix Albe, retired, from Institut Franco-Allemand de Recherches de Saint-Louis for their collaboration for developing the transmission and reflection holographic interferometers. A great thank also to Professor Pascal Picart from Laboratoire d'Acoustique du Maine for the implementation of digital holographic interferometry in ONERA. The section 6 of this research has been funded from the French National Agency for Research (ANR) under grant agreement n° ANR 2010 BLAN 0302.

9. References

Bjelkhagen, H.I. & Vukicevic, D. (1992). Lippmann color holography in single-layer silver-halide emulsion, *5th International Symposium On Display Holography*, T. H. Jeong ed. Proc. SPIE Vol.2333, pp. 34-48

Bjelkhagen, H.I. (1993). Silver-halide recording-materials for holography and their processing, *Springer Series in Optical Sciences*, Vol.66, Springer Verlag New-York, ISBN 3-540-58619-9.

Bjelkhagen H.I., Jeong, T.H. & Vukicevic, D. (1996). Color reflection holograms recorded in a panchromatic ultra high-resolution single-layer silver-halide emulsion", *Journal of Imaging Sciences and Technology*, Vol.40, pp. 134-146

Bjelkhagen, H.I. & Mirlis, E. (2008). Color holography to produce highly realistic three-dimensional images, *Applied Optics*, Vol.47, pp. A123-A133

Cha, D.J. & Cha, S.S. (1996). Holographic interferometric tomography for limited data reconstruction, *AIAA Journal*, Vol.34, pp. 1019-1026

Demoli, N., Vukicevic, D. & Torzynski, M. (2003). Dynamic digital holographic interferometry with three wavelengths, *Optics Express*, Vol.11, pp. 767-774.

Desse, J.M. (1990). Instantaneous density measurement in two-dimensional gas flow by high speed differential interferometry, *Experiments in Fluids*, Vol.9, pp. 85-91

Desse, J.M. (1997a). Recording and processing of interferograms by spectral characterization of the interferometric setup, *Experiments in Fluids*, Vol.23, pp. 265-271

Desse, J.M. (1997b). Three-color differential interferometry, *Applied Optics*, Vol.36, pp. 7150-7156

Desse, J.M. (2006). Recent contribution in color interferometry and applications to high-speed flows, *Optics and Lasers in Engineering*, Vol.44, pp. 304-320

Desse, J.M., Picart, P. & Tankam, P. (2008). Digital three-color holographic interferometry for flow analysis, *Optics Express*, Vol.16, pp. 5471-5480

Desse, J.M., Picart, P. & Tankam, P. (2010). Digital Three-Color Holographic Interferometry Devoted to Fluid Mechanics, *Optical metrology*, Speckle 2010 7387, 73870S1-73870S6

Ferraro, P., De Nicola, S., Coppola, G., Finizio, A., Alfieri, D. & Pierattini, G. (2004). Controlling image size as a function of distance and wavelength in Fresnel-transform reconstruction of digital holograms, *Optics Letters*, Vol.29, pp. 884-886

Ferraro, P., Miccio, L., Grilli, S., Paturzo, M., De Nicola, S., Finizio, A., Osellame, R. & Laporta, P. (2007). Quantitative phase microscopy of microstructures with extended measurement range and correction of chromatic aberrations by multi wavelength digital holography, *Optics Express*, Vol.15, pp. 14591-14600

Fomin, N. (1998). Speckle photography for fluid mechanics measurements, *Springer*, Berlin Heidelberg New York, ISBN: 978-3-540-63767-7

Fomin, N., Lavinskaya, E. & Vitkin, D. (2002). Speckle tomography of turbulent flows with density fluctuations, *Experiments in Fluids*, Vol.33, pp. 160-169

Harthong, J., Sadi, J., Torzynski, M. & Vukicevic, D. (1997). Speckle phase averaging in high-resolution color hologhraphy, *Journal of the Optical Society of America A*, Vol.14, pp. 405-410.

Hubel, P.M. (1991). Recent advances in color reflection holography, *Practical Holography V*, S.A. Benton ed. Proceeding SPIE Vol.1461, pp. 167-174

Javidi, B., Ferraro, P., Hong, S., De Nicola, S., Finizio, A., Alfieri, D. & Pierattini, G. (2005). Three-dimensional image fusion by use of multiwavelength digital holography, Optics Letters, Vol.30, pp. 144-146

Jeong, T.H., Bjelkhagen, H.I. & Spoto, L.M. (1997). Holographic interferometry with multiple wavelengths, *Applied Optics*, Vol. 36, pp. 3686-3688

Joannes, L., Dupont, O., Dubois, F., Colinet, P. & Legros, J.C. (2000). Interferometric optical tomography for 3-dimensional investigation of liquids, In: Carlomagno GM, Grant I (eds) CD ROM *Proceedings of the 8th International Symposium on Flow Visualization*, Edinburgh, Heriot Watt, Scotland, pp. 428.1-428.9

Kato, J., Yamaguchi, I. & Matsumura, T. (2002). Multicolor digital holography with an achromatic phase shifter, *Optics Letters*, Vol.27, pp. 1403-1405.

Kim, J.M., Choi, B.S., Choi, Y.S., Kim, J.M., Bjelkhagen, H.I. & Phillips, N.J. (2002). Holographic Optical Elements Recorded in Silver Halide Sensitized Gelatin Emulsions. Part 2. Reflection Holographic Optical Elements, *Applied Optics*, Vol.41, pp. 1522-1533

Kuhn, J., Colomb, T., Montfort, F., Charrière, F., Emery, Y., Cuche, E., Marquet, P. & Depeursinge, C. (2007). Real-time dual-wavelength digital holographic microscopy with a single hologram acquisition, *Optics Express*, Vol.15, pp. 7231-7242

MacAdam, D.L. (1985). Color Measurement, *Springer Series in Optical Sciences*, Vol.27, Springer Verlag Berlin Heidelberg, ISBN 0-387-15573-2

Merzkirch, W. (1965). A simple schlieren interferometer system, *AIAA Journal,* Vol.3, pp. 1974-1976

Merzkirch, W. (1974). Flow visualization, *Academic Press New York*, ISBN 0-12-491350-4

Picart, P., Moisson, E., Mounier, D. (2003). Twin sensitivity measurement by spatial multiplexing of digitally recorded holograms, *Applied Optics*, Vol.42, pp. 1947-1957.

Picart, P., Leval, J., Grill, M., Boileau, J.P., Pascal, J.C., Breteau, J.M., Gautier, B. & Gillet, S. (2005). 2D full field vibration analysis with multiplexed digital holograms, *Optics Express*, Vol.13, pp. 8882-8892

Pellicia-Kraft, B.J. & Watt, D.W. (2000). Three-dimensional imaging of a turbulent jet using shearing interferometry and optical tomography, *Experiments in Fluids*, Vol.29, pp. 573-581

Pellicia-Kraft, B.J. & Watt, D.W. (2001). Visualization of coherent structure in scalar fields of unsteady jet flows with interferometric tomography and proper orthogonal decomposition, *Experiments in Fluids*, Vol.30, pp. 633-644

Petrova, T.S., Ivanov, B., Zdravkov, Z., Nazarova, D., Stoykova, E., Minchev, G. & Sainov, V. (2009). Basic Holographic Characteristics of a Panchromatic Light Sensitive Material for Reflective Autostereoscopic 3D Display, *EURASIP Journal on Advances in Signal Processing*, Vol. 2009, Article ID 217341

Philbert, M. (1958). Emploi de la strioscopie interférentielle en aérodynamique, *La Recherche Aérospatiale*, Vol.65, pp. 19-27

Rastogi, P.K. (1994). (Ed.) Holographic interferometry, principles and methods, *Springer Series in Optical Sciences*, Vol.68, Springer Verlag Berlin Heidelberg, ISBN 0-387-57354-2

Sasomov, Y., Kumonko, P., Ratcliffe, D., Skokov, G. & Grichine, M. (1999). Recent advances in holographic materials from Slavich, *Holographic materials V*, T.J. Trout ed. Proceeding SPIE Vol. 3638, pp. 42-53

Settles, G.S. (2001). Schlieren and shadowgraph techniques, *Springer-Verlag*, Berlin Heidelberg New-York, ISBN 3-540-66155-7

Smeets, G. ((1975). Observational techniques related to differential interferometry, In: *Proceeding of 11th International Congress on High Speed Photography*, Chapman & Hall, UK, pp. 283-288

Smigielski, P., Fagot, H. & Albe, F. (1976). Application de l'holographie ultra rapide à référence arrière à l'étude de déformations dynamiques, *Proceeding of the 12th International Congress of High Speed Photography*, Toronto

Surget, J. (1973). Etude quantitative d'un écoulement aérodynamique, *La Recherche Aérospatiale*, Vol.3, pp. 167-171

Timmerman, B. & Watt, D.W. (1995). Tomographic high-speed digital holographic interferometry, *Measurement Science and Technology*, Vol.6, pp. 1270-1277

Vest, C.M. (1979). Holographic interferometry, *Wiley-Interscience*, ISBN 0-471-90683-2, New-York

Vikram, C.S. & Witherow, W.K. (1992). Critical needs of fringe order accuracy in two-colour holographic interferometry", *Experiments in Mechanics*, pp. 74-77

Yamaguchi, I. & Zhang, T. (1997). Phase-shifting digital holography, *Optics Letters*, Vol.22 pp. 1268-1270

Yamaguchi, I., Matsumura, T. & Kato, J. (2002). Phase-shifting color digital holography, *Optics Letters*, Vol.27, pp. 1108-1110.

Yan, D. & Cha, S.S. (1998). Computational and interferometric system for real-time limited-view tomography of flow fields, *Applied Optics*, Vol.37, pp. 1159-1164

Zhao, J., Jiang, H. & Di, J. (2008). Recording and reconstruction of a color holographic image by using digital lensless Fourier transform holography, Optics Express, Vol.16, pp. 2514-2519.

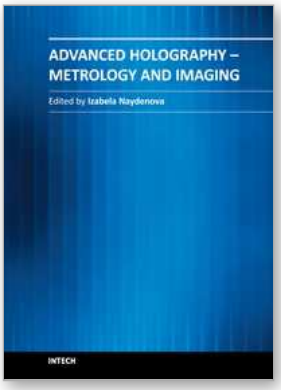

Advanced Holography - Metrology and Imaging

Edited by Dr Izabela Naydenova

ISBN 978-953-307-729-1
Hard cover, 374 pages
Publisher InTech
Published online 09, November, 2011
Published in print edition November, 2011

Advanced Holography - Metrology and Imaging covers digital holographic microscopy and interferometry, including interferometry in the infra red. Other topics include synthetic imaging, the use of reflective spatial light modulators for writing dynamic holograms and image display using holographic screens. Holography is discussed as a vehicle for artistic expression and the use of software for the acquisition of skills in optics and holography is also presented. Each chapter provides a comprehensive introduction to a specific topic, with a survey of developments to date.

How to reference

In order to correctly reference this scholarly work, feel free to copy and paste the following:

Jean-Michel Desse (2011). Real-Time Colour Holographic Interferometry (from Holographic Plate to Digital Hologram), Advanced Holography - Metrology and Imaging, Dr Izabela Naydenova (Ed.), ISBN: 978-953-307-729-1, InTech, Available from: http://www.intechopen.com/books/advanced-holography-metrology-and-imaging/real-time-colour-holographic-interferometry-from-holographic-plate-to-digital-hologram-

INTECH
open science | open minds

InTech Europe
University Campus STeP Ri
Slavka Krautzeka 83/A
51000 Rijeka, Croatia
Phone: +385 (51) 770 447
Fax: +385 (51) 686 166
www.intechopen.com

InTech China
Unit 405, Office Block, Hotel Equatorial Shanghai
No.65, Yan An Road (West), Shanghai, 200040, China
中国上海市延安西路65号上海国际贵都大饭店办公楼405单元
Phone: +86-21-62489820
Fax: +86-21-62489821